JOURNAL OF MATERIALS SCIENCE 31 (1996) 1789–1796

Vapour deposited cone formation during fabrication of low voltage field emitter array cathodes

D. N. HILL, J. D. LEE, J. K. COCHRAN, A. T. CHAPMAN
School of Materials Science and Engineering, Georgia Institute of Technology, Atlanta, GA 30332-0245, USA

A line-of-sight vapour deposition process is used to form a low-voltage field emission cathode structure on the surface of an oxide–metal eutectic composite etched to expose arrays of single-crystal tungsten fibres. A SiO_2 insulating film is first deposited, forming cone-shaped deposits on the tips of the exposed fibres. These cones act as a shadow mask for the subsequent deposition of a metal film. After removal of the cones, the metal film forms a grid-like structure with concentric apertures centered on each fibre tip. Application of a potential of less than 100 V between the metal grid and the base of the fibres produces an electric field at the fibre tips of sufficient intensity to produce field emission. The equilibrium geometry of the deposits which form on the fibre tips (cathode cones) is such that there is a linear relationship between the height of the cone and its diameter. There is also a direct correlation between the cathode cone angle, which depends on the material being deposited, and the cone angle of the insulator film. For SiO_2, the cathode cone angle was determined to be 37°, while the cone angle of the insulator film was 26°. Comparison of the theoretical values of the lateral growth velocity of the cathode cones with values determined from experimental measurements indicated that the maximum sticking coefficient was independent of the growth angle, η, for SiO_2, but varied as a function of $\cos \eta$ for molybdenum. A multiple deposition process was developed which permitted independent control of the interelectrode spacing and insulator film thickness.

1. Introduction

The drive toward high-brightness, flat-screen displays, and the continuing demand for high-current-density electron sources, both for microwave and cathode ray tubes, has generated renewed interest in field emitter array (FEA) cathodes. These devices, with their potential for electron current densities orders of magnitude greater than oxide or dispenser cathodes, offer a number of other advantages over thermionic cathodes, not the least of which is cold operation.

A thin film field emitter array structure has been developed based on a directionally-solidified oxide–metal eutectic composite developed by Chapman and Clark [1]. This composite consists of arrays of parallel, single-crystal tungsten fibres, 300–1000 nm in diameter, growing longitudinally through a refractory oxide matrix, typically UO_2 or Y_2O_3-stabilized ZrO_2. The spatial density of fibres in the arrays typically range from $5–15 \times 10^6$ fibres cm^{-2}, depending on growth conditions. Descriptions of the unique process by which the composites are formed appear in the literature, and the reader is referred there for details [2, 3].

The thin film FEA structure, based on a concept originally developed by Spindt [4], consists of an array of refractory emitter elements surrounded by a concentric metal anode, which is in turn supported by a dielectric film that insulates it from the substrate. Due to the small interelectrode spacing (typically less than 1 μm) and the field enhancement provided by the sharp radius of the emitting tip, a relatively small potential applied to the extractor produces an electric field at the pin tip sufficient to cause emission of electrons *in vacuo*. Simultaneous, parallel operation of an array of these emitters is possible because they are electrostatically isolated from each other by the integral extractor electrode. High fibre packing densities provided by the eutectic composite structure give these devices the potential for significant current density levels relative to the thermionic cathodes in use today.

Unlike the Spindt-type structure, which uses vapour-deposited molybdenum cones as the emitter elements, the composite-based low voltage field emitter (LVFE) structure utilizes the tungsten fibres as the emitter elements and a unique deposition process to form the remainder of the structure. This structure, shown schematically in Fig. 1, consists of an array of free-standing metal fibres, each surrounded by a concentric metal electrode (extractor) in close proximity to the fibre tip.

The structure is formed by etching away the oxide matrix of the polished substrate to expose the tungsten fibres. A metal oxide (insulator film) is then evaporated onto the substrate containing the exposed fibres.

0022-2461 © *1996 Chapman & Hall*

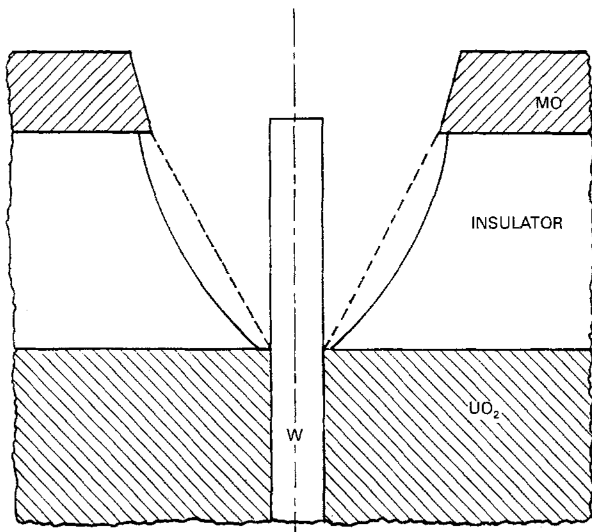

Figure 1 Schematic diagram of an individual emitter element of a low voltage field emitter array.

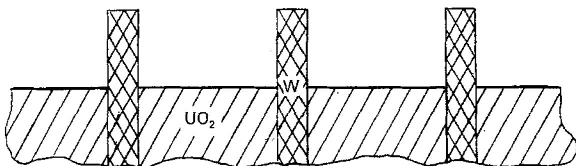

Step 1. Etch a polished oxide-metal composite to produce free-standing metal fibres (cathodes).

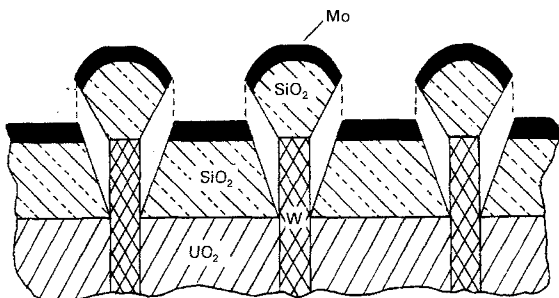

Step 2. Vapour deposit SiO_2 and Mo parallel to the fibre axes to the desired thickness.

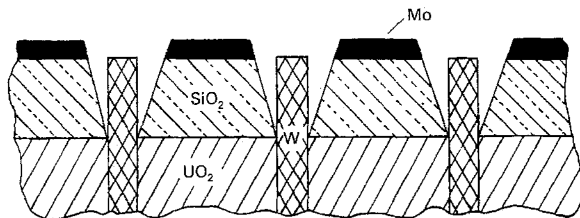

Step 3. Remove the cathode cones and clean remanent SiO_2 from the cathode using a combination of HF acid etch and ultrasonic vibration.

Figure 2 Schematic diagram illustrating the steps in the fabrication of a field emitter array cathode.

Line-of-sight deposition parallel to the fibre axis causes cone-shaped deposits to form on the tips of the exposed fibres. These cones then act as a shadow mask for the subsequent deposition of the metal extractor grid, thus allowing the grid to be placed in close proximity to the tips of the exposed fibres. The steps in the formation of the LVFE structure are illustrated in the series of diagrams in Fig. 2, and examples of the actual structure at each stage of the process are presented in the series of photomicrographs in Fig. 3. Details of the fabrication process for the LVFE cathode, can be found in the literature [5,6].

In this paper we examine a key element in the fabrication of the composite-based gridded structure: the formation of the cone-shaped deposits on the tips of the emitter pins which provide the shadow mask for deposition of the metal extractor grid. Although a variety of both insulator and conductive extractor materials appear usable for forming the desired geometry, SiO_2 and molybdenum were selected for study in this investigation. SiO_2 is attractive as an insulator film because of its excellent dielectric properties, while molybdenum offers favourable deposition and etching characteristics. Both materials also

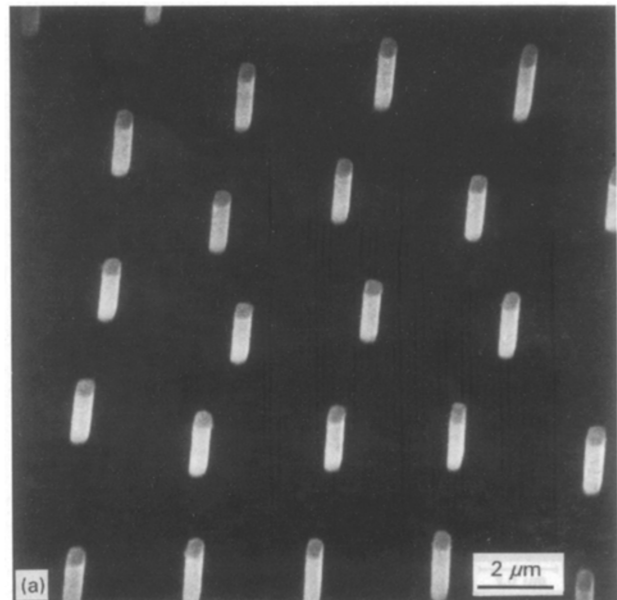

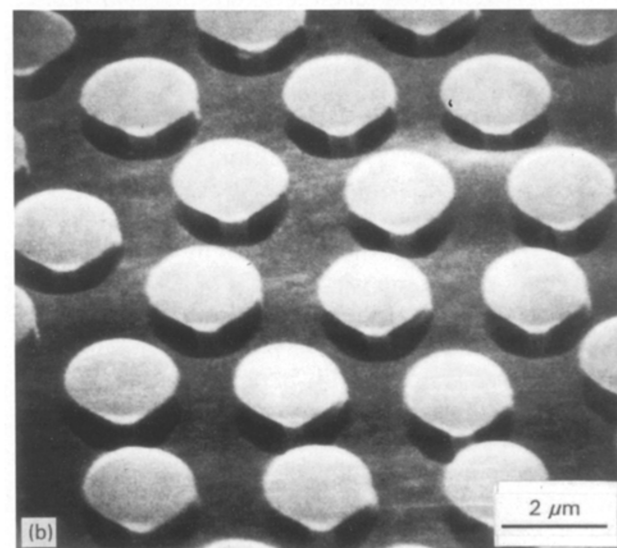

Figure 3 Photomicrographs of the LVFE structure, corresponding to each of the fabrication steps in Fig. 2, (a) after etching the UO_2–W eutectic composite to expose the fibres, (b) after deposition of the SiO_2 and Mo films, (c) the appearance of the structure after removal of the cathode cones.

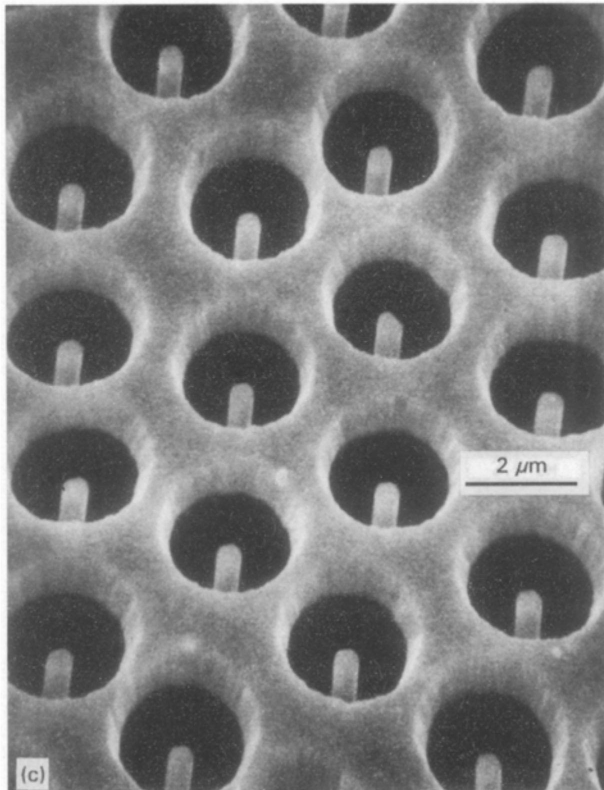

Figure 3 (Continued)

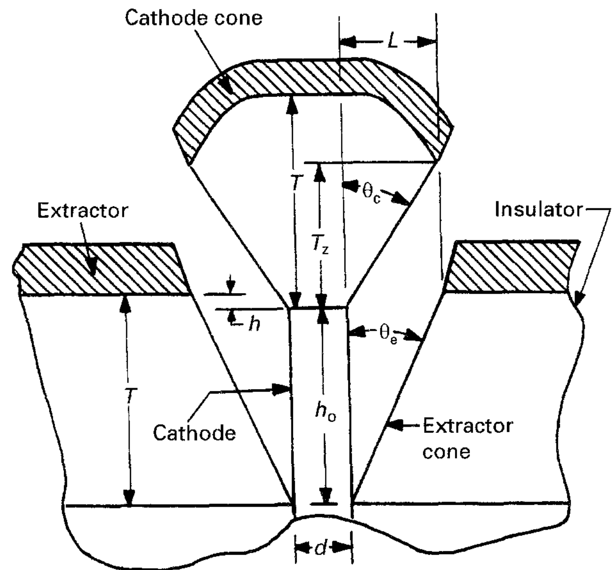

Figure 4 Schematic diagram showing the parameters used to define the LVFE structure.

exhibit low mobility on the substrate during deposition, an essential attribute for proper formation of the structure.

2. Experimental procedure

The composites are normally grown in the form of ingots 20–30 mm in diameter and 70–80 mm high. The ingots were sliced perpendicular to the growth direction using a slow-speed cut-off saw with a diamond blade. The resulting wafers, 1–2 mm thick, were cemented to a glass plate and cylindrical chips 4.2 mm in diameter were cut from the wafers with a diamond core drill. After removing the glass backing, the chips were polished to a 300 nm finish on a diamond lap.

The chips were etched to expose the tungsten fibres to the desired length and shape the tips. Using five samples, with fibres 1–1.5 μm in length, SiO_2 layers were deposited at room temperature, at a rate of $30\ nm\ min^{-1}$, to five different thicknesses up to 1.0 μm, using a step shutter which allowed masking of successive samples as film thickness increased. A thin layer (20–30 nm) of molybdenum was deposited over the SiO_2 to provide a conductive film for SEM examination. The cathode cones were removed using a combination of HF etching and ultrasonic vibration. In a similar manner, five samples were polished and coated with molybdenum films in order to measure the dimensions of the resulting molybdenum cones.

2.1. Measurement of cone characteristics

The geometry resulting from the line-of-sight deposition process was controlled by the deposition characteristics of the thin film structure on the tungsten fibre tips. In order to evaluate the process, the cathode cone was defined using parameters which could be geometrically related to the emitter structure, as shown in Fig. 4. The LVFE geometry can be defined in terms of the insulator film thickness, T, the interelectrode spacing, L, (the distance between the vertical axis at the side of a tungsten pin and the edge of the extractor hole), and the position of the fibre tip, h, relative to the plane of the insulator–extractor interface.

The interelectrode spacing, L, was determined from measurements of the extractor hole diameter and fibre diameter in photomicrographs taken at a viewing angle of less than 3°. The value of L was calculated from the relation

$$L = (D - d)/2 \qquad (1)$$

where D is the extractor hole diameter and d is the fibre diameter. The effect of the viewing angle on the measurement was negligible at the 3° viewing angle. The height of the fibre tip above the matrix, h_0, was measured in the SEM for each cathode after etching of the matrix was completed and prior to deposition of the insulator film.

The diagram shown in Fig. 5 illustrates the technique used to determine the remaining characteristics of the LVFE structure. The cathode cone angle, θ_c, measured relative to the fibre axis, was calculated from the viewing angle, ϕ, and the various dimensions labelled l_1, l_2 and l_3 in Fig. 5. Note that l_2 and l_3 are measured in a plane perpendicular to the fibre axis, while l_1 is measured in a plane angled at θ_c degrees from the fibre axis. From Fig. 5:

$$\sin(\phi - \theta_c) = l_2/c \qquad (2)$$

and

$$c = l_1/\sin\phi \qquad (3)$$

Combining Equations 2 and 3,

$$\theta_c = \phi - \sin^{-1}[(l_2/l_1)/\sin\phi] \qquad (4)$$

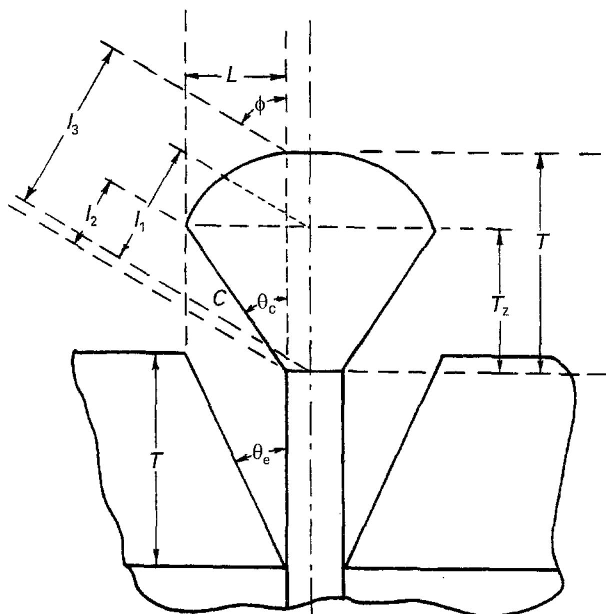

Figure 5 Schematic diagram illustrating the technique used to measure cone dimensions in the SEM.

The insulator film thickness, T, and the vertical component of the cone at the shadowing edge, T_z, are given by:

$$T = l_3/\sin\phi \quad (5)$$

and

$$T_z = l_1(\cos\theta_c)/\sin\phi \quad (6)$$

In several cases, the SiO_2 film thickness was also measured at the edge of a fracture surface; these values typically agreed with the measurements taken from the cathode cones within ± 0.1 μm. The cone angle of the extractor cone, θ_e, is determined by the relation between the extractor–cathode spacing at the insulator–extractor interface, L, and the insulator thickness, T, or

$$\theta_e = \tan^{-1}(L/T) \quad (7)$$

The cathode cones shown in the photomicrographs of Fig. 6 are typical of those used to obtain the values of l_1–l_3.

2.2. Two-stage deposition

The advantage of being able to independently vary the insulator thickness, T, and extractor-cathode spacing, L, led to the development of a "two-stage deposition" process. The steps in this process are illustrated in Fig. 7. After completion of the initial deposition, the sample is taken from the vacuum chamber and the cathode cones are removed from the fibre tips by ultrasonic vibration. After etching away high-surface-area SiO_2 deposits with dilute HF, the sample is returned to the vacuum chamber and a second SiO_2 film is deposited. During the second deposition, as the cathode cone grows outward from the fibre tip, the SiO_2 extractor cone diameter decreases until the cathode cone shadows the extractor cone a second time (Fig. 7c). Thus, the SiO_2 insulator thickness can be

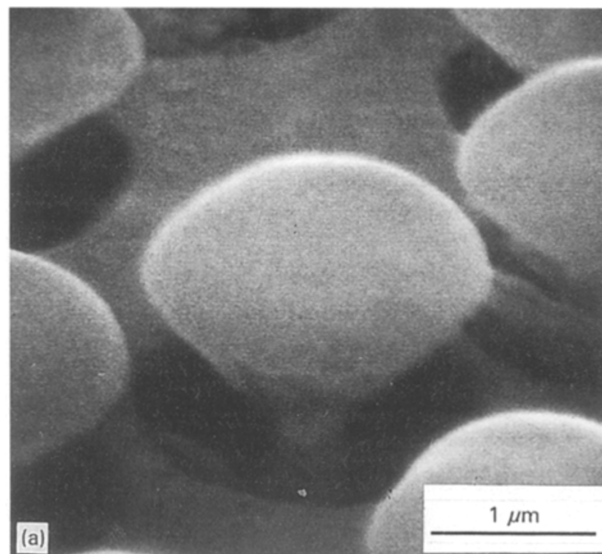

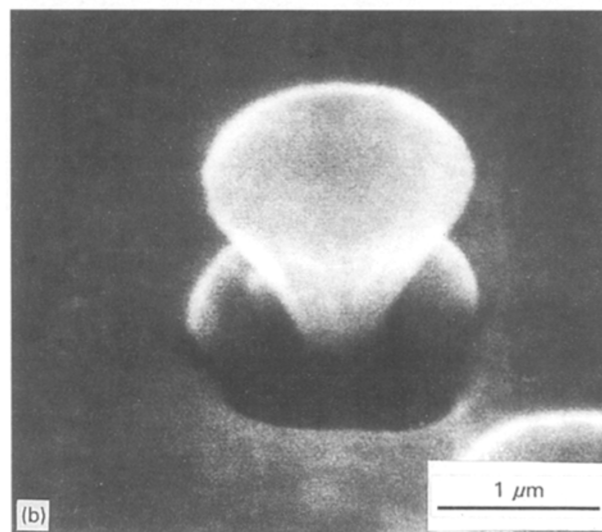

Figure 6 Typical examples of cathode cones used to measure the cone dimensions, (a) SiO_2 and (b) Mo.

increased while decreasing the extractor–cathode spacing.

In order to determine the relation between the interelectrode spacing, L', and the film thickness, T, that resulted from the two-stage deposition process, five samples were prepared in a manner similar to that used for the single-deposition experiments. The five samples were initially coated with a SiO_2 film 0.75 μm thick, the cathode cones were removed, and secondary films ranging in thickness from 0.2 to 1.0 μm were deposited.

3. Results and discussion

3.1. Single deposition

The ratio of the vertical and horizontal components of the cathode cone (at the shadowing edge) to the film thickness, $X_v = T_z/T$ and $X_l = L/T$, respectively, are the characteristics which, together with the fibre spacing, control the cathode geometry; and hence ultimately determine the geometric limitations of the LVFE structure. The values of X_l, X_v, θ_c, and θ_e,

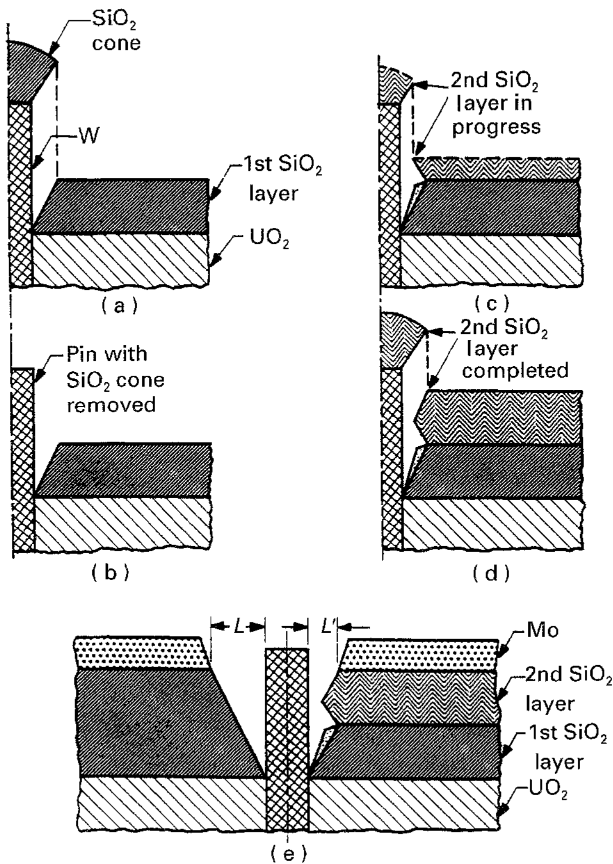

Figure 7 Schematic diagram illustrating the steps in the two-stage deposition process.

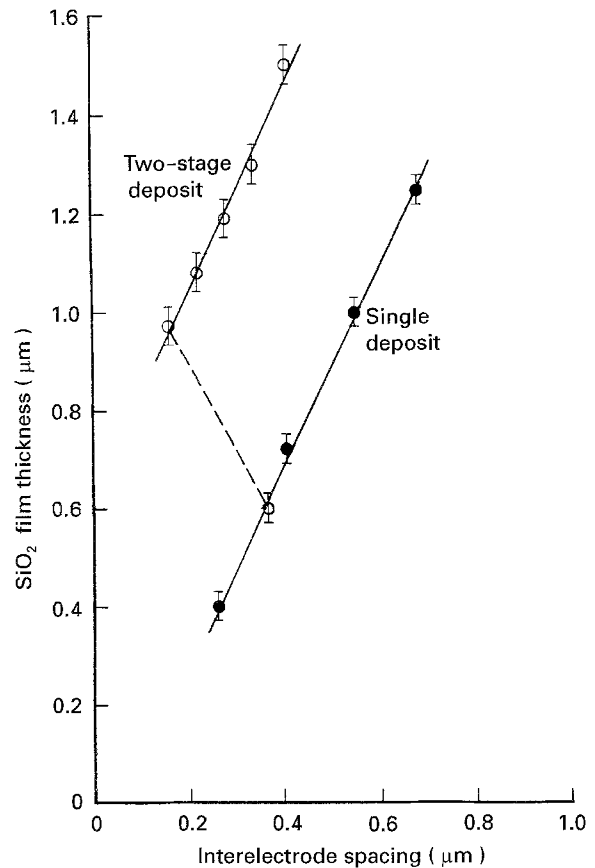

Figure 8 Plots of insulator film thickness versus interelectrode spacing, illustrating the effectiveness of the two-stage deposition process for maintaining small interelectrode spacings while increasing SiO_2 film thickness.

TABLE I Characteristics of SiO_2 and Mo cathode cones

Parameter	SiO_2	Mo
$X_l(L/T)$	0.49	0.36
$X_v(T_z/T)$	0.65	0.70
θ_c	37°	27°
θ_e	26°	20°

calculated from measurements of the cathode cones in the SEM, are listed in Table I for both SiO_2 and Mo.

Referring to Fig. 5, one can see that the cathode cone angle, θ_c, can also be defined by the relation

$$\theta_c = \tan^{-1}(L/T_z) \quad (8)$$

Since the shadow from the growing cathode cone forms the extractor cone cavity, the geometry of the cathode cone controls the geometry of the extractor. Furthermore, comparing Equations 7 and 8, it is evident that the cathode cone angle, θ_c, will always be larger than the extractor cone angle, θ_e. This results from the fact that, in order to preserve the cone shape, T_z must always be less than the cone thickness above the fibre tip, the value of which is equal to the insulator film thickness, T.

The position of the cathode tip relative to the insulator–extractor interface, h, is defined as

$$h = h_o - T \quad (9)$$

Note that h is positive when the cathode tip is above the insulator–extractor interface and negative when the tip is below the interface (Fig. 4). The maximum negative value of h (the maximum distance the cathode tip could be placed below the extractor) corresponds to the film thickness, T_{max}, that is just sufficient to cause the extractor cone to intercept the cathode cone. This occurs when

$$T_{max} = h_o + T_{z_{max}} \quad (10)$$

The vertical component, T_z, is equal to $0.65T$ for SiO_2 (Table I), so that

$$T_{max} = h_o + 0.65T_{max} \quad (11)$$

or,

$$T_{max} = 2.85h_o \quad (12)$$

Thus, for a given pin height, h_0, a SiO_2 insulating film could not exceed a thickness of 2.85 times the pin height without the risk of the cathode cone growing to the edge of the insulator film and closing the hole.

Plots of the interelectrode spacing as a function of insulator film thickness for both the single- and two-stage deposition experiments are shown in Fig. 8. For the single deposition experiments, the values of interelectrode spacing and extractor film thickness could be fit to an equation of the form:

$$L = 0.49T + T_o \quad (13)$$

where the values of L, T, and T_0 are expressed in micrometres. The fact that the value of T_0 was non-zero was a result of non-linear growth on the tungsten

fibre tip prior to the cone forming an equilibrium shape; it appeared to be somewhat dependent on the fibre tip geometry. For the cylindrical tips in this study it was ≈ 0.06 μm. The extractor cone angle, calculated from the slope of the line was found to be $\approx 26°$. This compares with a value of $\approx 27°$ calculated from direct measurements of the cathode cones. Hence the lateral growth of the extractor cone produced an interelectrode spacing that was ≈ 50 per cent of the SiO_2 insulator thickness.

3.2. Two-stage deposition

The extractor geometry obtained after two-stage deposition is illustrated schematically in Fig. 7e. As expected, for the two-stage deposition process, the SiO_2 hole diameter decreased until the cathode cone reshadowed the insulator cone edge. The hole became irregularly shaped prior to reshadowing, but after reshadowing had occurred, the hole became circular again. Reshadowing was observed to occur at a secondary deposit thickness approximately half the thickness of the initial deposit. This comes as no surprise, since the extractor cone wall grows toward the cathode (prior to its being reshadowed) by the same mechanism that produces the cathode cone. Note that the slopes of the two plots of interelectrode spacing as a function of film thickness are essentially the same (Fig. 8); hence, the interelectrode spacing after the second deposition is approximately equal to a material-specific constant (tan θ_e) multiplied by the thickness of the secondary deposit, neglecting the effect of the initial irregular growth on the fibre tip. This assumes that the thickness of the second deposit is sufficient for re-shadowing to have occurred. Clearly, deposition of the extractor film would be impractical until after reshadowing had occurred; otherwise, the insulating film would be shorted by deposition of the metallic extractor film.

The extractor hole diameter is plotted as a function of SiO_2 insulator film thickness for both the single- and two-stage deposition experiments in Fig. 9. This plot indicates that the practical upper limit of film thickness for the SiO_2 film is ≈ 2.5 μm for a single deposition, since the hole diameter at that thickness approaches typical fibre separation distances for fibre packing densities of 1.0×10^7 cm^{-2}, i.e. ≈ 3 μm. Comparison of the two plots clearly shows that the SiO_2 film thickness can be doubled while still maintaining the same extractor hole diameter and interelectrode spacing. This could be extremely useful for reducing the capacitance of an LVFE cathode for high-frequency applications. The effect of two-stage deposition on the extractor hole diameter is illustrated in the series of photomicrographs in Fig. 10.

3.3. Cathode cone formation

Examination of the cathode cone parameters defined in Fig. 5 allows one to deduce the material characteristics which control the shape of the cones. If there were no surface diffusion during deposition, i.e. no atomic surface mobility, every accepted molecule

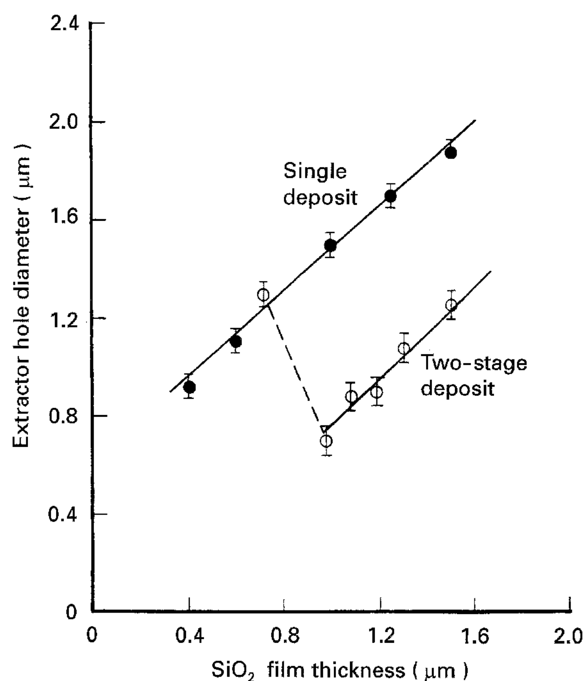

Figure 9 Plots of extractor hole diameter as a function of insulator film thickness for the single and two-stage deposition processes.

would stick in the location where it landed, a faceted crystal shape would be lost, and the film would grow only in the direction of the beam. The final texture would be determined by the deposition angle, η, and molecule sticking coefficient, A [7]. In general, the value of A has been assumed by previous investigators to be either independent of η, proportional to cos η, or proportional to sin η [4].

It is evident from Fig. 6 that the final shape of the film deposited on the tips of the tungsten fibres is that of an expanding cone rather than a continuous film growing only in the beam direction, that the cones grow linearly with film thickness, and that the cone angle is a function of the material being deposited. Silicon dioxide films prepared by electron beam evaporation are known to be amorphous, and molybdenum films prepared below 400 °C have been shown to be polycrystalline with a grain size of less than 40 nm [8]. As is evident from the cathode cones pictured in Fig. 6 there were no crystal facets or evidence of crystalline grains on the cone surfaces. It is safe to assume the atomic mobility of SiO_2 and Mo is extremely low, considering the high melting points of the materials and the use of unheated substrates. Therefore, it is reasonable to assume that the SiO_2 and Mo films were deposited with negligible surface diffusion.

The deposition angle, η, between the beam direction and the normal to the substrate surface increases continually from zero at the center of the fibre tip to 90° at the edge (Fig. 11). The film growth velocity in the direction normal to the deposit surface is determined by the angle η and the sticking coefficient, A. In order for a film to grow, it must be exposed to the molecular flux from the source. Areas on the substrate which have a deposition angle less than that corresponding to the maximum lateral growth velocity will

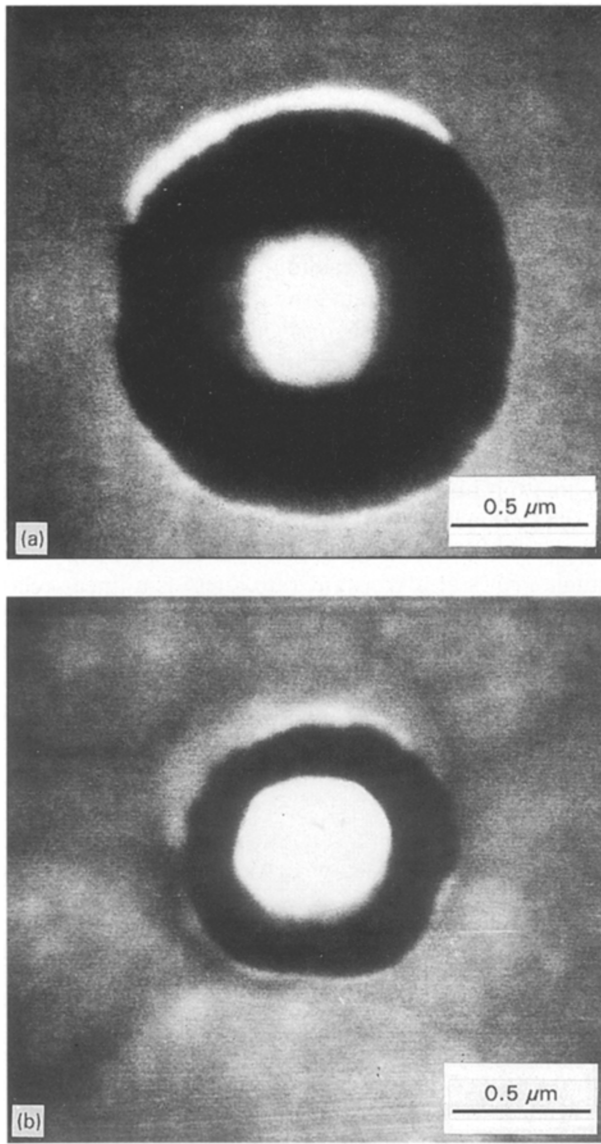

Figure 10 Photomicrographs of emitter elements from two LVFE cathodes having approximately the same insulator film thickness, (a) single deposit and (b) two-stage deposit.

continue to grow. However, the growth velocities normal to the substrate surface vary with the deposition angle, decreasing continually from the centre of the cones to the edge. This results in spontaneously changing deposition angles associated with each new surface geometry. The surface geometry continues to change until an equilibrium cone edge geometry is formed. After forming an equilibrium edge, the film edge grows linearly at a constant angle to the deposition direction, resulting in the formation of the cathode cones illustrated in Fig. 6. This equilibrium angle, η_c, is the cathode cone angle (Fig. 11).

The equilibrium geometry of the growing cathode cone is determined by a combination of the molecular sticking coefficient, A, and the critical angle, η_c, which is the deposition angle corresponding to the vertical and lateral growth velocity of the edge of the cathode cone. The film growth relative to a normal surface in the critical angle direction is given by (refer to Fig. 11):

$$T_{\eta_c}/T = A \cos \eta_c \quad (14)$$

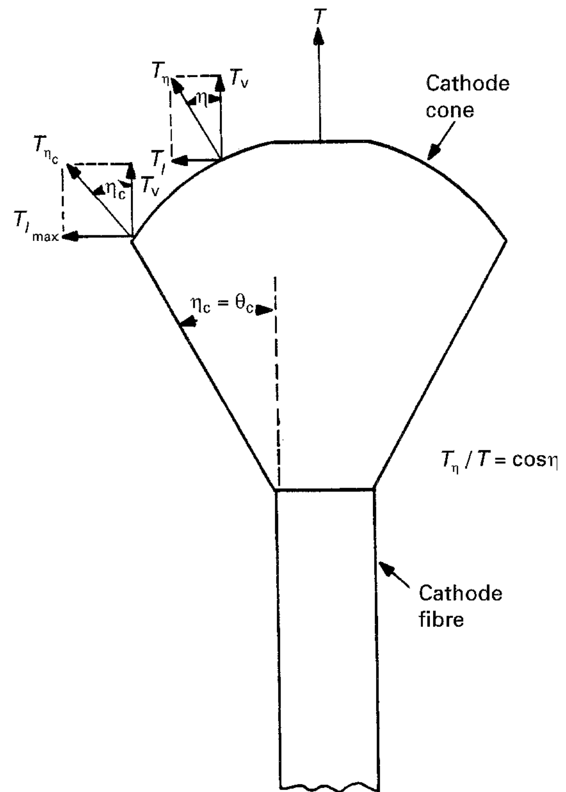

Figure 11 Schematic diagram of a cathode cone, illustrating the variation in T_l as the deposition angle v_c increases.

where T_{η_c}/T is the ratio of firm thickness at η_c to a normal deposit. Hence, the equilibrium lateral and vertical growth velocities of the cone edge, v_l, and v_v, are given by:

$$v_l = T_l/T = A \cos \eta_c \sin \eta_c \quad (15)$$

and

$$v_v = T_v/T = A \cos^2 \eta_c \quad (16)$$

Dividing Equation 22 by Equation 23 gives,

$$\eta_c = \tan^{-1} (v_l/v_v) \quad (17)$$

The relative lateral and vertical growth velocities of the edge of the cathode cone are equilibrium values and as such, should be equivalent to the experimental parameters X_l and X_v described previously. Using the values for these parameters listed in Table I, η_c was calculated for SiO_2 and Mo from Equation 17. From the resulting values of η_c, values for v_l and v_v were calculated from Equations 15 and 16, assuming $A = 1$. The results of these calculations are listed in Table II.

As can be seen from the table, X_l agreed very well with v_l and X_v with v_v for SiO_2. However, to provide similar agreement for molybdenum, A had to be assumed to be equal to $\cos \eta$. Thus the molecular sticking coefficient for SiO_2 appears to be independent of η, while that for molybdenum is proportional to $\cos \eta$.

The maximum lateral relative growth rate, $(v_l)_{max}$, will occur at a deposition angle η_{max}. For SiO_2, assuming $A = 1$,

$$v_l = \cos \eta \sin \eta, \quad (18)$$

TABLE II Deposition parameters for the formation of SiO_2 and Mo cones

Parameter	SiO_2	Mo
v_l $(A = 1)$	0.49	0.41
v_l $(A = \cos\eta)$	–	0.36
v_v $(A = 1)$	0.62	0.79
v_v $(A = \cos\eta)$	–	0.70
η_c	38°	27°
η_{max}	45°	35°
$(v_l)_{max}$	0.50	0.38

and

$$d(v_l)/d\eta = \sin^2\eta - \cos^2\eta \qquad (19)$$

At η_{max}, $d(v_l)/d\eta = 0$ and $\eta_{max} = 45°$. Thus $(v_l)_{max} = 0.50$. For molybdenum, assuming $A = \cos\eta$,

$$(v_l) = \cos^2\eta \sin\eta \qquad (20)$$

and $\eta_{max} = 35.3°$, giving a value of $(v_l)_{max}$ of 0.38 (Table II). The values of $(v_l)_{max}$ and X_l were quite close for both SiO_2 and molybdenum assuming $A = 1$ for SiO_2 and $A = \cos\eta$ for molybdenum. This suggests that the maximum lateral growth velocity at the edge of the cone varies little from the equilibrium growth rate of the cone edge.

As one might expect, based on earlier arguments, the calculated value of η_{max} is greater than the measured value of η_c (or θ_c) for both SiO_2 and Mo. This is due to the fact that, while the lateral relative growth velocity varies only slightly from the equilibrium value at the growing edge of the cone, the vertical growth velocity at the shadowing edge will always be less than the equilibrium value of v_v because of the sharp change in the deposition angle at that point.

4. Conclusions

A technique for the formation of a low voltage field emitter array cathode utilizes line-of-sight deposition of a low-mobility insulating material onto etched, free-standing tungsten fibres. This results in the formation of cone-shaped deposits on the tips of the fibres, which then act as a mask for the subsequent deposition of a metallic film. When the cones are removed, the metallic film forms a gridded structure with each fibre tip centred in the apertures of the grid.

The geometry of the growing cones is determined by a combination of the molecular sticking coefficient and the deposition angle (measured relative to the deposition direction) corresponding to the equilibrium vertical and lateral growth velocity of the edge of the cone. The deposition angle (cathode cone angle) was found to be a function of the material being deposited. The maximum lateral growth velocity of the edge of the cone was found to be approximately equal to the equilibrium growth rate of the cone edge. Comparison of the theoretical values of the lateral growth velocity of the cathode cones with values determined from experimental measurements indicated that the maximum sticking coefficient was independent of the growth angle for SiO_2, but varied as a function of $\cos\eta$ for molybdenum.

The geometry of the cathode cone controls the cone angle of the insulator film. Since the cathode cone angle grows at a constant rate, there is a linear relationship between the extractor hole diameter (and thus the interelectrode spacing) and the insulator film thickness. A multiple deposition process permits independent control of the insulator film thickness and interelectrode spacing.

References

1. A. T. CHAPMAN and G. W. CLARK, *J. Amer. Ceram. Soc.* **48** (1965) 494.
2. A. T. CHAPMAN, J. K. COCHRAN, J. F. BENZEL, R. K. FEENEY, F. W. LING and J. D. NORGARD, Final Technical Report, DARPA Contract DAAH01-70-C-1057, December, 1973.
3. A. T. CHAPMAN, J. K. COCHRAN, R. K. FEENEY and D. N. HILL, Final Technical Report, Army MICOM Contract DASHO1-75-C-0852, December, 1977.
4. C. A. SPINDT, *J. Appl. Phys.* **47** (1976) 5248.
5. J. K. COCHRAN, A. T. CHAPMAN, R. K. FEENEY and D. N. HILL, Final Technical Report, Army MRDC Contract DAAK40-77-0096, January, 1979.
6. J. K. COCHRAN, A. T. CHAPMAN, R. K. FEENEY, D. N. HILL, K. J. LEE, R. D. JONES, R. V. KOLARIK, K. H. MOH, and J. P. PRICE, Final Technical Report, Air Force Wright Aeronautical Lab. Contract AFWAL-TR-82-1089, July, 1982.
7. A. VAN DER DRIFT, *Philips Res. Rep.* **22** (1967) 267.
8. H. OIKAWA, *J. Vac. Sci. Tech.* **14** (1977) 1153.

Received 2 August 1994
and accepted 15 August 1995